






BRIEF DEFINITIVE REPORT

ACKR4 restrains antitumor immunity by regulating CCL21

Carly E. Whyte¹, Maleika Osman¹, Ervin E. Kara¹, Caitlin Abbott¹, Jade Foeng¹, Duncan R. McKenzie¹, Kevin A. Fenix¹, Yuka Harata-Lee¹, Kerrie L. Foyle¹, Sarah T. Boyle², Marina Kochetkova², Amelia Roman Aguilera³, Jijie Hou³, Xian-Yang Li³, Mark A. Armstrong⁴, Stephen M. Pederson⁴, Iain Comerford^{1*}, Mark J. Smyth^{3*}, and Shaun R. McColl^{1*}

Current immunotherapies involving CD8⁺ T cell responses show remarkable promise, but their efficacy in many solid tumors is limited, in part due to the low frequency of tumor-specific T cells in the tumor microenvironment (TME). Here, we identified a role for host atypical chemokine receptor 4 (ACKR4) in controlling intratumor T cell accumulation and activation. In the absence of ACKR4, an increase in intratumor CD8⁺ T cells inhibited tumor growth, and nonhematopoietic ACKR4 expression was critical. We show that ACKR4 inhibited CD103⁺ dendritic cell retention in tumors through regulation of the intratumor abundance of CCL21. In addition, preclinical studies indicate that ACKR4 and CCL21 are potential therapeutic targets to enhance responsiveness to immune checkpoint blockade or T cell costimulation.

Introduction

Immune checkpoint inhibitors have revolutionized the therapeutic landscape for treatment of malignancies, with objective clinical responses observed in a proportion of many cancers, particularly those in which tumor mutational burden is high or immune gene signatures are favorable (Ahern et al., 2018; Chen and Mellman, 2017). A major determinant for patient outcome is the extent of CD8⁺ T cell infiltration of the tumor, and increased intratumor CD8⁺ T cell frequency is correlated with improved anti-PD-1/PD-L1 responsiveness in melanoma (Herbst et al., 2014; Tumei et al., 2014) and improved outcomes in colorectal cancer regardless of treatment (Galon et al., 2006; Pagès et al., 2009). Thus, understanding molecular cues that govern CD8⁺ T cell entry and accumulation in tumors is paramount to developing new therapies that may act in concert with established treatments to improve clinical efficacy. Tumor-specific CD8⁺ T cells are primarily thought to be primed in draining LNs (dLNs) by the Batf3-dependent lineage of CD103⁺ conventional dendritic cells (DCs), which are capable of efficient transport of tumor-derived antigen to the LN and subsequent cross-presentation to CD8⁺ T cells (Broz et al., 2014). Once primed, expression of CXCR3 by effector CD8⁺ T cells enables their recruitment into the tumor microenvironment (Mikucki et al., 2015), where in the absence of expression of inhibitory molecules, such as

PD-1, they can mediate tumor destruction. This CD8⁺ T cell recruitment is thought to be largely controlled by CD103⁺ DCs at the tumor site, which have been shown to be the predominant source of the ligands CXCL9 and CXCL10 in multiple tumors (de Mingo Pulido et al., 2018; Spranger et al., 2017). Thus, via their control of multiple facets of the CD8⁺ T cell response, CD103⁺ DCs are a key determinant of the magnitude of the antitumor response, and understanding their regulation in tumor settings is of great therapeutic importance.

Migration of tumor antigen-bearing CD103⁺ DCs to dLNs and subsequent priming of tumor-specific CD8⁺ T cells are highly dependent on CCR7, and in human melanoma, expression of CCR7 is positively correlated with both T cell infiltration and patient survival (Broz et al., 2014; Roberts et al., 2016). Moreover, there is a significant body of evidence implicating CCR7 in varied facets of the biology of tumors of many different origins (Boyle et al., 2016; Haniffa et al., 2012; Wang et al., 2005). The atypical chemokine receptor 4 (ACKR4) has emerged as an important regulator of CCR7, as it binds to the CCR7 ligands CCL19 and CCL21 as well as the CCR9 ligand CCL25. This fails to induce classical GPCR signaling and chemotaxis and instead leads to chemokine degradation (Comerford et al., 2006, 2010; Townson and Nibbs, 2002). By controlling chemokine bioavailability and

¹Chemokine Biology Laboratory, Department of Molecular and Biomedical Science, School of Biological Sciences, The University of Adelaide, Adelaide, South Australia, Australia; ²Centre for Cancer Biology, University of South Australia and SA Pathology, Adelaide, South Australia, Australia; ³Immunology in Cancer and Infection Laboratory, QIMR Berghofer Medical Research Institute, Brisbane, Queensland, Australia; ⁴Bioinformatics Hub, School of Biological Sciences, The University of Adelaide, Adelaide, South Australia, Australia.

*I. Comerford, M.J. Smyth, and S.R. McColl contributed equally to this paper; Correspondence to Shaun R. McColl: shaun.mccoll@adelaide.edu.au.

© 2020 Crown copyright. The government of Australia, Canada, or the UK ("the Crown") owns the copyright interests of authors who are government employees. The Crown Copyright is not transferable. This article is distributed under the terms of an Attribution-Noncommercial-Share Alike-No Mirror Sites license for the first six months after the publication date (see <http://www.rupress.org/terms/>). After six months it is available under a Creative Commons License (Attribution-Noncommercial-Share Alike 4.0 International license, as described at <https://creativecommons.org/licenses/by-nc-sa/4.0/>).

maintaining functional chemotactic gradients, ACKR4 has been shown to regulate migration of DCs into lymphatics as well as T cell areas of LNs (Bryce et al., 2016; Heinzl et al., 2007; Ulvmar et al., 2014). Despite the importance of CCR7 signaling in tumor settings, the role of ACKR4 in controlling tumor immunity has been largely unexplored. Studies of ACKR4 in tumor settings have been predominantly limited to transgenic expression in immunodeficient mouse models, and the contribution of endogenously expressed ACKR4 to antitumor immunity is unknown (Feng et al., 2009; Harata-Lee et al., 2014; Shi et al., 2015). In this study, we aimed to determine if host ACKR4 contributes to malignant progression and whether it plays a role in shaping antitumor immunity.

Results and discussion

ACKR4 regulates tumor growth in multiple mouse models

To begin to investigate a potential role for ACKR4 in influencing tumor progression, *Ackr4*^{-/-} mice were interbred with mice harboring the MMTV-PyMT transgene, which recapitulates the step-wise progression and distinct morphological features of human breast cancer (Fantozzi and Christofori, 2006; Lin et al., 2003). The development of palpable tumors was significantly delayed and total tumor burden at 20 wk of age was significantly reduced in PyMT⁺ *Ackr4*^{-/-} compared with PyMT⁺ *Ackr4*^{+/+} (PyMT⁺B6) mice (Fig. 1, A and B). To support this finding, we inoculated WT or ACKR4-deficient mice with either intermediate (25 μg) or high (300 μg) doses of 3-methylcholanthrene (MCA) to induce fibrosarcoma (Ngiow et al., 2016). *Ackr4*^{-/-} mice displayed a significant survival advantage compared with WT mice (Fig. 1, C and D). Finally, in the orthotopic E0771 mammary carcinoma model, an established model of triple-negative, basal-like breast cancer (Denkert et al., 2017; Johnstone et al., 2015), growth of tumors was significantly impaired in ACKR4-deficient mice compared with WT controls (Fig. 1, E and F). Thus, deletion of ACKR4 inhibits tumor growth in multiple tumor models.

Ackr4^{-/-} mice develop enhanced tumor-specific CD8⁺ T cell responses

Given the importance of the CCR7 axis in immune homeostasis, we hypothesized that the altered tumor growth in ACKR4-deficient mice was a result of alterations in tumor-infiltrating lymphocytes. Analysis of tumors on day 21 after inoculation demonstrated a significant increase in CD44^{hi} CD8⁺ T cells in E0771 tumors from *Ackr4*^{-/-} mice compared with WT mice (Fig. 2 A), with no alteration in other major lymphocyte populations (Fig. S1, A–D). There was a significant increase in IFN-γ-expressing CD8⁺ T cells from *Ackr4*^{-/-} mice upon restimulation ex vivo as well as increased IFN-γ on a per-cell basis (Fig. 2 B), indicative of enhanced effector function, although the frequency of granzyme B expression was unaltered (Fig. 2 C and Fig. S2 E). Expression of PD-1 on CD8⁺ T cells was also modestly increased in *Ackr4*^{-/-} mice, although TIM-3 and LAG-3 expression was unaltered (Fig. 2, D–F; and Fig. S2, F and G). Coexpression of PD-1 with LAG-3 or TIM-3, previously suggested to be indicative of a highly dysfunctional CD8⁺ T cell

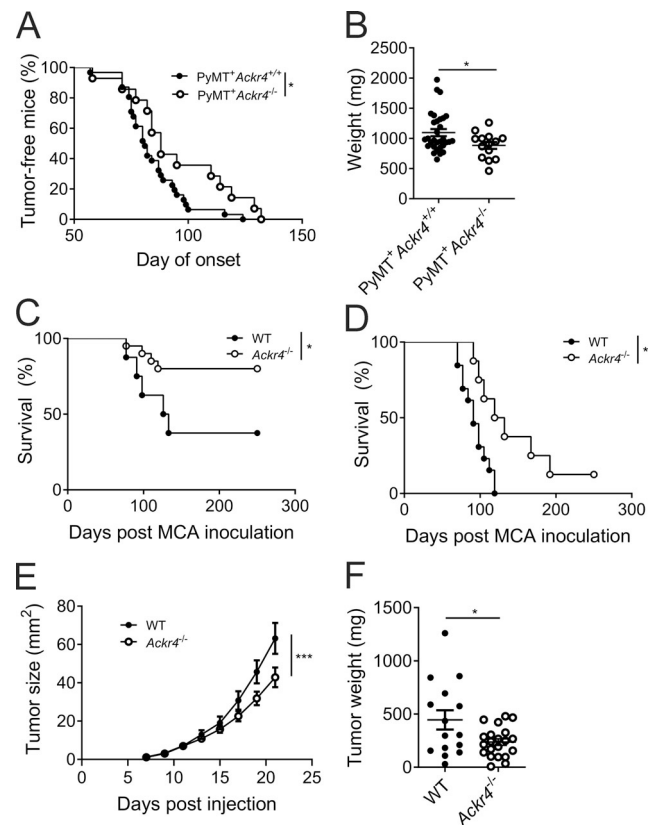


Figure 1. Loss of ACKR4 inhibits tumor growth in vivo. (A) Age of tumor onset for MMTV-PyMT B6 (*Ackr4*^{+/+}) and *Ackr4*^{-/-} mice; *n* = 31 (*Ackr4*^{+/+}), 14 (*Ackr4*^{-/-}), Mantel-Cox test. (B) Total weight of mammary glands in MMTV-PyMT B6 and *Ackr4*^{-/-} at 20 wk of age; *n* = 31 (*Ackr4*^{+/+}), 14 (*Ackr4*^{-/-}), unpaired *t* test. (C and D) Survival curve of WT and *Ackr4*^{-/-} mice inoculated with 25 μg (C) or 300 μg (D) MCA in the hind flank (C: *n* = 8, 20; D: *n* = 13, 8, Mantel-Cox test). (E and F) Growth curves (E) and weights (F) of WT or *Ackr4*^{-/-} mice injected with 10⁵ E0771 mammary carcinoma cells. Data in E and F are pooled from three independent experiments; *n* = 16–21 (E, two-way ANOVA; F, unpaired *t* test). Data are presented as mean ± SEM. *, *P* ≤ 0.05; ***, *P* ≤ 0.001.

phenotype (Fourcade et al., 2010; Kurtulus et al., 2019; Matsuzaki et al., 2010; Sakuishi et al., 2010; Woo et al., 2012), was also unaltered (Fig. 2 G and Fig. S2, H and I). This suggests that these intratumor CD8⁺ T cells are somewhat more activated in *Ackr4*^{-/-} mice than those in WT mice but are not fully dysfunctional, indicating they may be more amenable to PD-1 blockade

To test if CD8⁺ T cells were responsible for the reduced tumor growth in *Ackr4*^{-/-} mice, WT and *Ackr4*^{-/-} mice were administered depleting anti-CD8β antibodies (Fig. 2 H). Depletion of CD8⁺ T cells from WT mice had no effect on E0771 tumor growth. However, depletion of CD8⁺ T cells from *Ackr4*^{-/-} mice significantly enhanced tumor growth, with tumors reaching similar sizes to that seen in WT mice. To compare tumor-specific CD8⁺ T cell responses more precisely, WT and *Ackr4*^{-/-} mice were injected with an E0771 cell line expressing the model antigen ovalbumin (E0771-OVA) to allow subsequent detection of OVA_{SIINFEKL}-specific CD8⁺ T cells by tetramer staining. At day 11 after injection with E0771-OVA cells, there was an increased number of OVA_{SIINFEKL}-specific

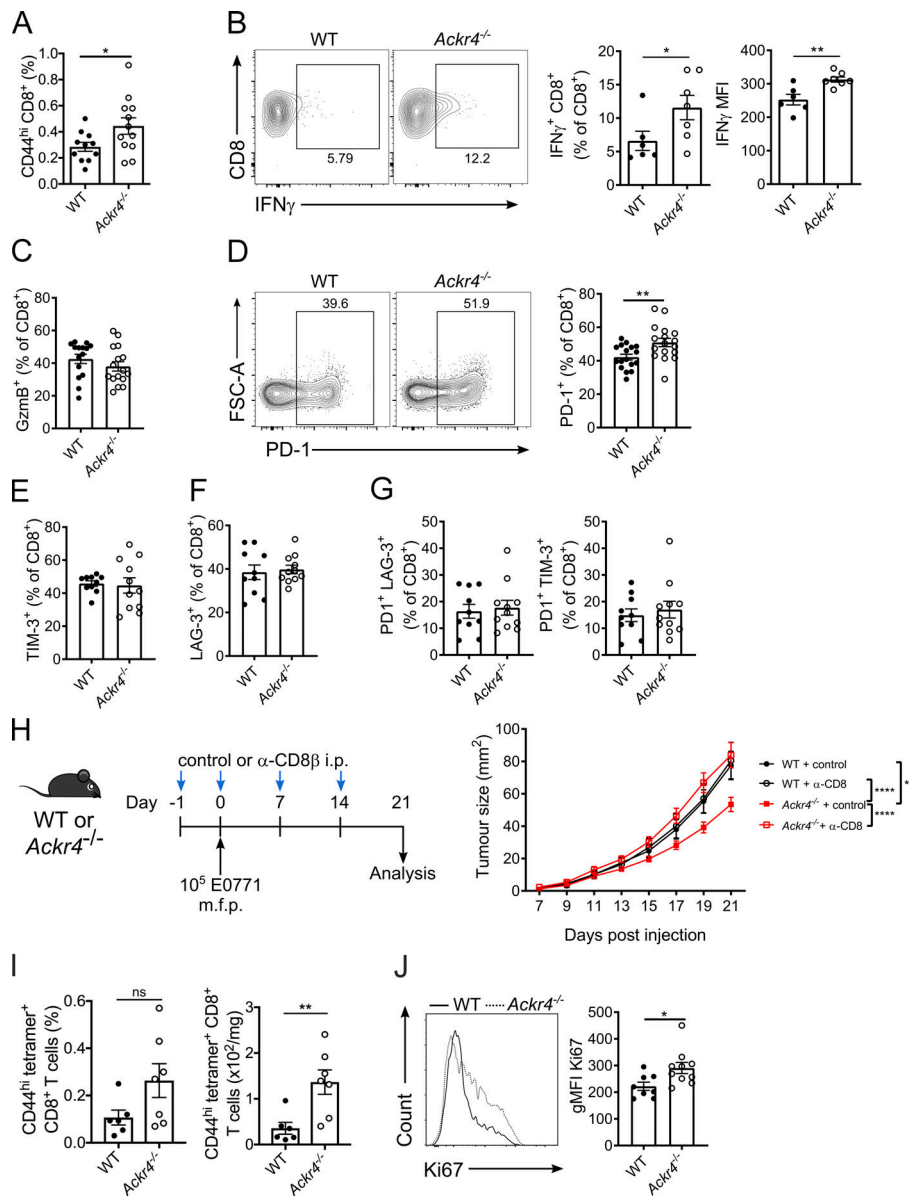


Figure 2. ACKR4-deficient mice mount an enhanced antitumor CD8⁺ T cell response. (A–G) WT or *Ackr4*^{-/-} mice were injected with 10⁵ E0771 cells and analyzed 18–21 d after injection. (A) Frequency of CD44^{hi} CD8⁺ T cells (of total viable cells) in tumors; *n* = 11–13, unpaired *t* test. MFI, mean fluorescence intensity. (B) Frequency of IFN-γ expression in intratumor CD8⁺ T cells and MFI of IFN-γ CD8⁺ T cells; *n* = 6–7, unpaired *t* test. (C and D) Frequency of granzyme B (C) or PD-1 expression (D) in intratumor CD8⁺ T cells; *n* = 17, unpaired *t* test. FSC-A, forward scatter area. (E–G) Frequency of TIM-3 (E), LAG-3 (F), PD-1⁺ TIM-3⁺ (G), or PD-1⁺ LAG-3⁺ expression in intratumor CD8⁺ T cells; *n* = 10–11. (H) WT or *Ackr4*^{-/-} mice were injected with E0771 cells and treated with 100 μg anti-CD8β depleting antibody or isotype control. Tumor growth curve; *n* = 9–14, two-way ANOVA. m.f.p., mammary fat pad. (I) Frequency (of total viable cells) and number of OVA-specific CD8⁺ T cells in E0771-OVA tumors; *n* = 6–7 mice, unpaired *t* test. (J) Representative flow cytometry and geometric mean fluorescence intensity (gMFI) of Ki67 on intratumor CD8⁺ T cells from mice injected with 10⁵ E0771 cells; *n* = 10, unpaired *t* test. Data are pooled (A, C, G, and H) or representative (B, I, and J) from at least two independent experiments (experiments shown in E–G were performed once). Data represent mean ± SEM; *, *P* ≤ 0.05; **, *P* ≤ 0.01; ***, *P* ≤ 0.0001; ns, *P* > 0.05.

CD8⁺ T cells in tumors from *Ackr4*^{-/-} mice, compared with WT controls (Fig. 2 I). Furthermore, a greater proportion of intratumor CD8⁺ T cells from *Ackr4*^{-/-} mice were undergoing proliferation in situ as indicated by expression of the proliferation marker Ki67 (Fig. 2 J and Fig. S1 J). In contrast, there was no difference in the quantity of tumor-specific CD8⁺ T cells in dLNs between *Ackr4*^{-/-} and WT mice (Fig. S1 K), indicating that their enhanced presence in tumors was not a consequence of increased priming of these cells in the LN. Furthermore, there was a significant decrease in Ki67 expression on CD8⁺ T cells from the dLN of *Ackr4*^{-/-} mice compared with WT mice (Fig. S1 L), in line with previous reports indicating that *Ackr4*^{-/-} mice show a defect in T cell priming in LNs (Comerford et al., 2010; Ulvmar et al., 2014). Together, these data reveal that despite defects in LN priming of tumor-specific CD8⁺ T cells, *Ackr4*^{-/-} mice have enhanced intratumor accumulation and proliferation of CD8⁺ T cells, resulting in reduced tumor growth.

Enhanced retention of CD103⁺ DCs in *Ackr4*^{-/-} tumors

Previous reports have demonstrated a role for ACKR4 in regulating DC trafficking to tissue-draining LNs (Bryce et al., 2016; Heinzl et al., 2007; Ulvmar et al., 2014). Given that CD103⁺ DCs express CCR7 upon maturation and are a critical regulator of antitumor CD8⁺ T cell responses (Broz et al., 2014; Roberts et al., 2016; Spranger et al., 2017), we hypothesized that loss of ACKR4 in tumor settings leads to dysregulation of CD103⁺ DC migration. In E0771 tumors grown in *Ackr4*^{-/-} mice, there was an increase in total Ly6C⁻ MHC-II⁺ CD11c⁺ DC frequency and number compared with WT (Fig. 3, A and B), as well as an increase in CD103⁺ DC numbers, although in line with previous reports these represented a small proportion of the overall DC infiltrate (Spranger et al., 2017; Fig. 3 C). The bulk of the DC infiltrate in E0771 tumors were the noncross-presenting CD172a⁺ cDC2 population, which were also increased in *Ackr4*^{-/-} mice (Fig. 3 D).

Conventional DCs, including CD103⁺ DCs, are known to rely on CCR7-mediated signaling for egress from tissues (Ohl et al., 2004;

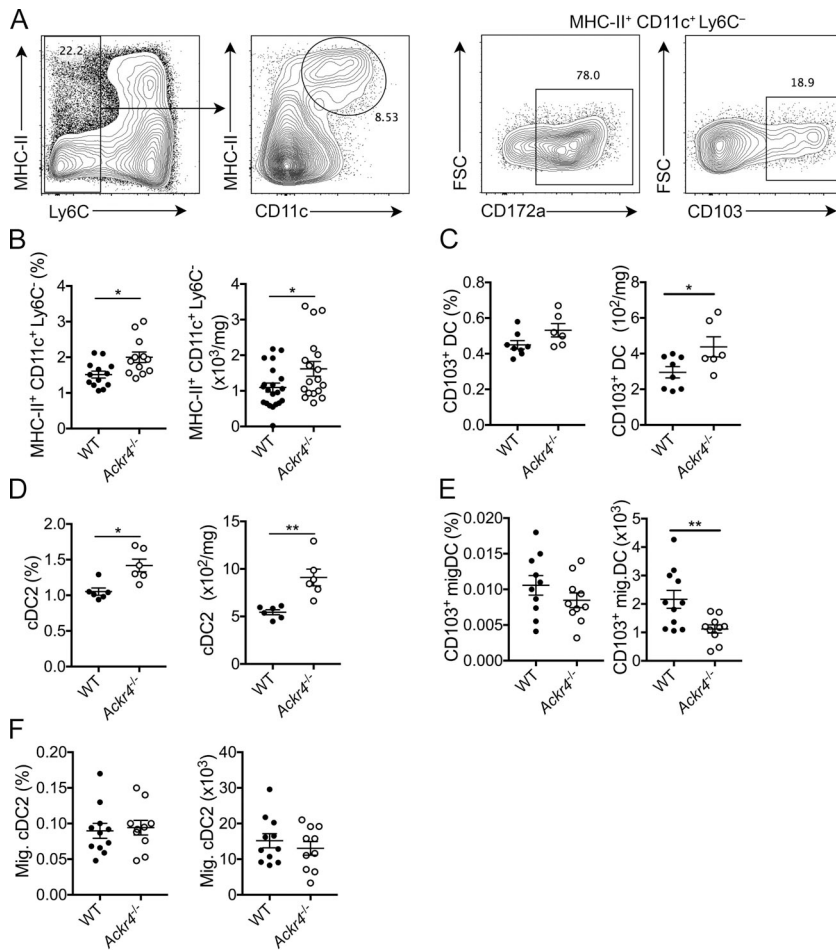


Figure 3. Loss of ACKR4 promotes intratumor DC accumulation. WT or *Ackr4*^{-/-} mice were injected with E0771 cells, and tumors were analyzed 18 d later. **(A)** Representative gating strategy for intratumoral DCs pregated on live CD45⁺ cells. FSC, forward scatter. **(B–D)** Frequency (of total viable cells) and number of intratumor (B) DCs (MHC-II⁺ CD11c⁺ Ly6C⁻), (C) CD103⁺ DCs, and (D) CD172a⁺ cDC2s. **(E and F)** Frequency and number of migratory (E) CD103⁺ DCs and (F) CD172a⁺ cDC2s in dLNs. Data are pooled from two independent experiments (B) or representative of at least two independent experiments (C–F); *n* = 6–10 mice, unpaired *t* test. Data are presented as mean ± SEM. *, *P* ≤ 0.05; **, *P* ≤ 0.01.

Roberts et al., 2016; Tal et al., 2011; Weber et al., 2013). Upon DC maturation, CCR7 expression is induced, which enables migration toward CCL21-expressing lymphatic vessels and subsequent tissue egress. Thus, it was also assessed whether the enhanced abundance of DC populations in tumors was coupled to a reduction in dLN numbers. There was a significant decrease in migratory CD103⁺ DC numbers in dLNs of *Ackr4*^{-/-} mice (Fig. 3 E), which along with their enhanced presence in tumors, suggested that CD103⁺ DCs displayed reduced capacity to egress from tumors to LNs in *Ackr4*^{-/-} mice. Migratory cDC2 numbers were unaltered in dLNs (Fig. 3 F), suggesting that the increased abundance of cDC2s in tumors in *Ackr4*^{-/-} hosts is not related to a defect in migration from tumor to LN. This difference in migration may reflect altered control of cDC2 egress compared with that of CD103⁺ DCs, a precedent being the recent observation that regulatory T cells can specifically hinder egress of cDC2, but not CD103⁺ DC from tumors (Binnewies et al., 2019), although these data do not rule out a role for increased recruitment of DCs into the tumor. Regardless, these data support a model whereby ACKR4 regulates migration of CD103⁺ DCs within the tumor microenvironment.

ACKR4 regulates DCs in tumors by controlling CCL21 abundance

ACKR4 expression has predominantly been reported on cells of nonhematopoietic origin (Heinzel et al., 2007; Lucas et al., 2015),

although we recently reported its expression on activated B lymphocytes (Kara et al., 2018). Therefore, to determine whether the effect of deletion of ACKR4 on tumor growth is mediated through the hematopoietic or stromal compartments or both, bone marrow (BM) chimeras were generated where ACKR4 deficiency was restricted to either the hematopoietic (*Ackr4*^{-/-} → WT) or nonhematopoietic (WT → *Ackr4*^{-/-}) compartments. E0771 tumor growth in chimeric mice lacking hematopoietic ACKR4 expression was unimpaired relative to WT chimeric controls (Fig. 4 A). However, nonhematopoietic deletion of ACKR4 was indispensable for the inhibited tumor growth seen in complete *Ackr4*^{-/-} mice.

Given that ACKR4 is a known scavenger of CCR7 ligands, we hypothesized that the alterations in tumor-infiltrating DCs were a result of aberrant regulation of these chemokines, akin to previously reported defects in DC egress from *Ackr4*^{-/-} skin (Bryce et al., 2016). We found a significant increase in CCL21 protein in E0771 tumors grown in *Ackr4*^{-/-} mice compared with WT mice (Fig. 4 B). While CCL25 was detected, there was no difference in its abundance between tumors grown in these strains, and CCL19 remained undetectable. The increased CCL21 within tumors grown in ACKR4-deficient mice implies that one or more cell types within the tumor stroma express ACKR4, controlling CCL21 abundance at this site. To test this, stromal populations (CD45⁻ mCherry⁻) from E0771mCherry tumors

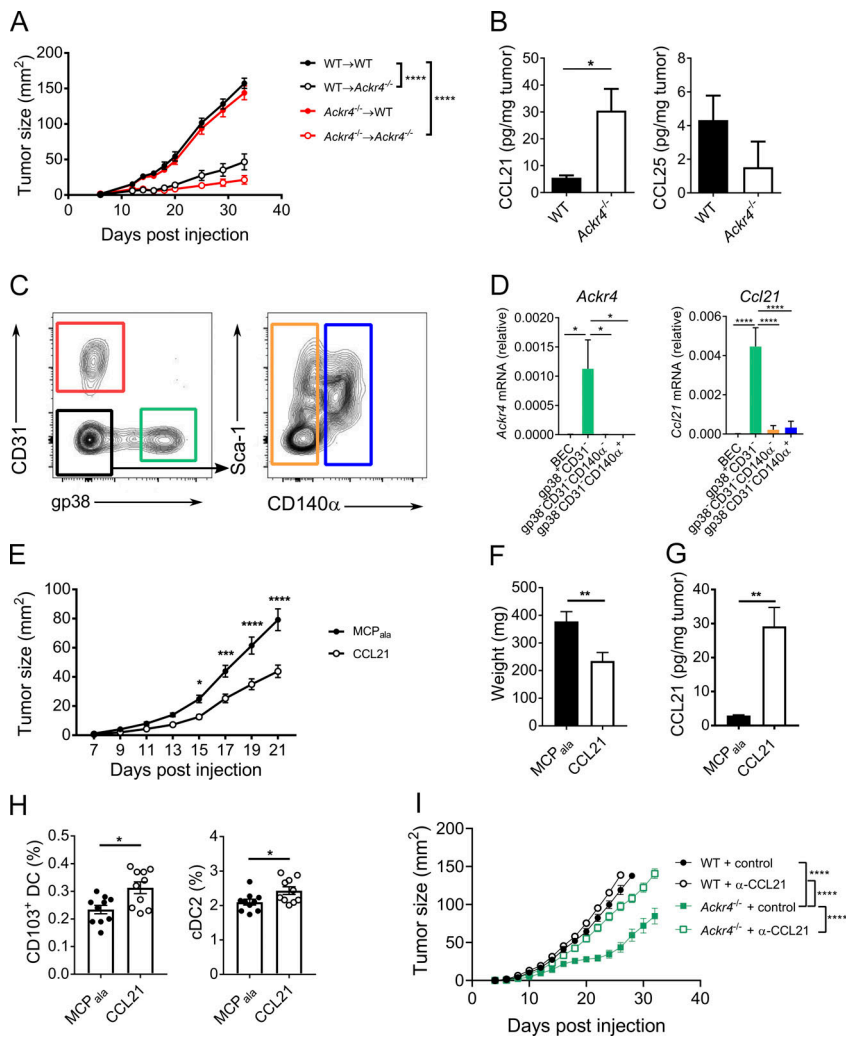


Figure 4. ACKR4 regulates CCL21 availability and enhances intratumor DC retention. (A) E0771 tumor growth in BM chimeras of WT and *Ackr4*^{-/-} mice (donor BM→host). Mice were injected with 5 × 10⁵ E0771 cells at least 8 wk after reconstitution; n = 9, two-way ANOVA. (B) CCL21 and CCL25 abundance in endpoint E0771 tumors; n = 6, unpaired t test. (C and D) *Ackr4* and *Ccl21* expression in stromal cells sorted from d13 E0771-mCherry tumors. (C) Representative gating strategy, pregated on CD45⁺ mCherry⁻ cells. (D) Relative expression of *Ackr4* and *Ccl21* by qPCR; n = 7, one-way ANOVA. (E–H) WT mice were injected with 10⁵ E0771 cells into contralateral sides of the inguinal mammary glands. MCP_{ala} or CCL21 (3 μg) was injected into contralateral glands every 3 d from the day of E0771 injection; n = 19 mice. (E) Tumor growth curves; two-way ANOVA. (F) Tumor weights at day 21 after injection; paired t test. (G) Intratumor CCL21 abundance; paired t test. (H) Frequency of intratumor CD103⁺ and CD172a⁺ cDC2s (of total viable cells); n = 10, paired t test. (I) E0771 tumor growth in WT and *Ackr4*^{-/-} mice treated with control or anti-CCL21 (100 μg) every 6 d from day -1; n = 6, two-way ANOVA. Data are representative (A, B, H, and I) or pooled (C–G) from at least two independent experiments. Data are presented as mean ± SEM. *, P ≤ 0.05; **, P ≤ 0.01; ***, P ≤ 0.001; ****, P ≤ 0.0001.

were sorted and analyzed for *Ackr4* expression by quantitative PCR (qPCR). Expression of *Ackr4* was restricted to gp38⁺ CD31⁻ fibroblasts (Fig. 4, C and D). Intriguingly, and in line with previous reports, these cells were also the major source of *Ccl21* (Peske et al., 2015). Fibroblasts in tumor environments are known to be heterogenous populations, with capability to both support and hinder antitumor responses (Costa et al., 2018; Turley et al., 2015). Thus, it is possible CCL21 production and its regulation through expression of ACKR4 is via distinct populations of fibroblasts.

To determine whether the enhanced retention of CD103⁺ DCs within the tumor and inhibition of tumor growth observed in *Ackr4*^{-/-} mice arose directly from excess CCL21, E0771 tumors were established in contralateral inguinal mammary glands in WT mice, and beginning from the day of E0771 injection, 3 μg CCL21 or the control peptide (MCP_{ala}) was administered every 3 d to each site of injection and into tumors once tumors were palpable. Administration of CCL21 led to a significant inhibition of tumor growth compared with MCP_{ala}-treated tumors (Fig. 4, E and F). Intratumor CCL21 levels achieved by exogenous dosing were similar to levels seen in *Ackr4*^{-/-} mice (Fig. 4 G). Furthermore, this was associated with a significant increase in both CD103⁺ DC and CD172a⁺ cDC2 abundance in these tumors

(Fig. 4 H). Finally, we confirmed that the reduced tumor growth observed in ACKR4-deficient mice was mediated through increased CCL21, as neutralization of CCL21 increased tumor growth to sizes similar to that of WT mice (Fig. 4 I). Thus, increased intratumor availability of CCL21 as a result of ACKR4 deletion directly enhanced accumulation of intratumor DCs.

Stromal ACKR4 promotes tumor metastasis

Next, it was assessed whether loss of ACKR4 also affected tumor metastasis. *Ackr4*^{-/-} mice showed reduced tumor colonization of the lung compared with WT mice when injected intravenously with B16 melanoma, 3LL lung carcinoma, or RM1 prostate carcinoma cells (Fig. S2, A–C). In a spontaneous metastasis model where E0771 primary tumors were resected at day 15, *Ackr4*^{-/-} mice also had enhanced survival compared with WT mice (Fig. S2 D). Mixed BM chimeras showed that loss of non-hematopoietic ACKR4 was both necessary and sufficient to inhibit lung metastasis in the B16 model (Fig. S2 E), suggesting a stromal source of ACKR4 regulates tumor lung colonization. In contrast to the CD8-mediated protection against E0771 tumor growth in ACKR4-deficient mice, protection in the intravenous B16 melanoma model is known to be largely mediated by natural killer (NK) cells (Saijo et al., 1984; Takeda et al., 2011). Thus, the

dependence of this phenotype on NK and CD8⁺ T cells was tested in metastasis in the E0771 model. Consistent with previous reports, CD8⁺ T cell depletion had no effect on the reduced metastasis observed in *Ackr4*^{-/-} mice compared with WT mice (Fig. S2 F). By contrast, depletion of NK cells or IFN- γ neutralization increased metastasis in both *Ackr4*^{-/-} mice and WT mice to an equivalent level. Thus, unlike in the primary tumor model, the enhanced protection against metastasis seen in ACKR4-deficient mice was dependent on NK cells, but not CD8⁺ T cells.

Loss of ACKR4 improves the efficacy of checkpoint inhibitors

Given that presence of intratumor CD8⁺ T cells in primary tumors is associated with increased responsiveness to immune checkpoint inhibitors (Tumeh et al., 2014), we assessed whether enhancing CD8⁺ responses through loss of ACKR4 also improved efficacy of immunotherapies. E0771 is relatively resistant to anti-PD-1 monotherapy (data not shown), but agonist monoclonal antibodies reactive with CD137 (4-1BB), a potent costimulatory molecule for T and NK cells (Chester et al., 2018; Melero et al., 1997), display antitumor activity against E0771 (Fig. 5 A). Treatment of WT mice bearing E0771 tumors with agonistic mAb against CD137 reduced tumor growth compared with control-treated mice; however, tumor growth was further inhibited in *Ackr4*^{-/-} mice treated with anti-CD137 mAb, indicating enhanced efficacy in the absence of ACKR4 (Fig. 5 A). To test whether the improved efficacy of anti-CD137 treatment was directly a result of increased CCL21, CCL21 (or a control MCP_{ala} peptide) was dosed in combination with anti-CD137 therapy. Indeed, exogenous administration of CCL21 significantly improved the efficacy of anti-CD137 (Fig. 5 B).

To test responsiveness to anti-PD-1 and anti-CTLA-4 combination therapy, we first employed the B16F10 melanoma model. There was a modest reduction in tumor growth in *Ackr4*^{-/-} mice treated with control antibody compared with equivalently treated WT mice (Fig. 5 C), indicating that loss of ACKR4 alone was not sufficient to greatly improve antitumor responses in all tumor types. Anti-PD-1/anti-CTLA-4 dual therapy reduced tumor burden; however, the extent of inhibition induced by combination therapy was significantly greater in *Ackr4*^{-/-} mice compared with their WT counterparts. Similar results were observed in the anti-PD-1-responsive MC38 colon adenocarcinoma model (Fig. 5 E). Anti-PD-1 mAb treatment was still significantly more effective in *Ackr4*^{-/-} mice than WT mice. Furthermore, anti-PD-1/anti-CTLA-4 combination therapy resulted in minimal tumor burden in *Ackr4*^{-/-} mice (seven out of eight tumors rejected) compared with WT mice (four out of eight tumors rejected). Intratumor administration of CCL21 also improved anti-PD-1/anti-CTLA-4 efficacy in both B16 and MC38 models in WT mice (Fig. 5, D and F). Finally, CCL21 neutralization in *Ackr4*^{-/-} mice treated with anti-PD-1/anti-CTLA-4 abrogated the improved response to immune checkpoint blockade (Fig. 5 G), indicating the protective effect of *Ackr4*^{-/-} mice is directly dependent on increased intratumor CCL21 abundance. Thus, in the absence of ACKR4, where there was an enhanced intratumor CD8⁺ T cell presence, multiple immunotherapies directed at increasing the quality of the T cell response showed enhanced efficacy.

ACKR4 correlated with reduced survival in stratified The Cancer Genome Atlas (TCGA) data

To assess whether this work may also be relevant in human breast cancer, we interrogated the TCGA database of RNA-sequencing data for primary breast carcinoma. Parsing tumors by a median split of *ACKR4* expression into high or low groups did not correlate with significant differences in overall patient survival (Fig. S3 A). However, we reasoned that reduced *ACKR4* expression may not be effective in inducing antitumor responses in “immune desert” tumors. Therefore, to enrich for tumors with an active immune response, samples were further parsed based on high expression of *CD8A*, *PRFI*, or *IFNG*. In these subgroups, there was a significant reduction in patient survival when tumors had high expression of *ACKR4* (Fig. S3, B–D).

In summary, we have shown here that *ACKR4* deficiency leads to inhibition of tumor growth in orthotopic, transgenic, and chemically induced models of cancer. The loss of *ACKR4* led to increased intratumor levels of CCL21, which was associated with an increase in CD103⁺ DC number in the tumor and enhanced accumulation and proliferation of intratumor CD8⁺ T cells, which were essential for the tumor control observed in *Ackr4*^{-/-} hosts. Furthermore, loss of *ACKR4* or intratumor CCL21 dosing enhanced responsiveness to multiple immunotherapies, suggesting targeting intratumor DCs through the *ACKR4*/*CCL21* axis may hold promise as a potential therapeutic target to complement existing approaches.

CD103⁺ DCs have considerable interest as a therapeutic target due to their many effects on enhancing antitumor CD8⁺ T cell responses (Broz et al., 2014; Hildner et al., 2008; Spranger et al., 2015, 2017). We show here that increasing CD103⁺ DCs at the tumor site, at the expense of their presence in dLN, is associated with a greater tumor-specific CD8⁺ T cell response and inhibited tumor growth, potentially due to increased intratumor recruitment and/or enhanced stimulation of primed CD8⁺ T cells that reach the tumor site, as evidenced by the enhanced expression of IFN- γ and Ki67 in intratumor CD8⁺ T cells from *ACKR4*-deficient mice. These observations additionally suggest that there is a threshold of DC trafficking required to initiate CD8⁺ T cell priming, which is still reached in the *Ackr4*^{-/-} mice, and subsequently tumor-residing DCs are more influential in the response than LN-residing DCs. More broadly, these results imply that therapies aimed at enhancing CD103⁺ DC frequency and activity specifically in the tumor will result in more beneficial outcomes.

This study provides rationale for two possible avenues for therapeutic intervention: inhibitory targeting of *ACKR4*, with subsequent effects on its three chemokine ligands, or, more specifically, exogenous administration of CCL21, with both approaches yielding beneficial outcomes here. The effects of *ACKR4* on tumor growth in this study seem to be mainly mediated through scavenging of CCL21 alone, and the results of intratumor CCL21 dosing build on previous studies demonstrating its efficacy (Sharma et al., 2000, 2003). The antitumor activity of CCL21 has previously been reported to be dependent on the CXCR3 ligands CXCL9 and CXCL10 (Sharma et al., 2003), which is consistent with the CXCR3-mediated recruitment of CD8⁺ T cells by intratumor CD103⁺ DC expression of these chemokines. Intriguingly, CCL21 has also been shown to be a ligand for CXCR3 in microglial cells (Rappert et al., 2002; Soto

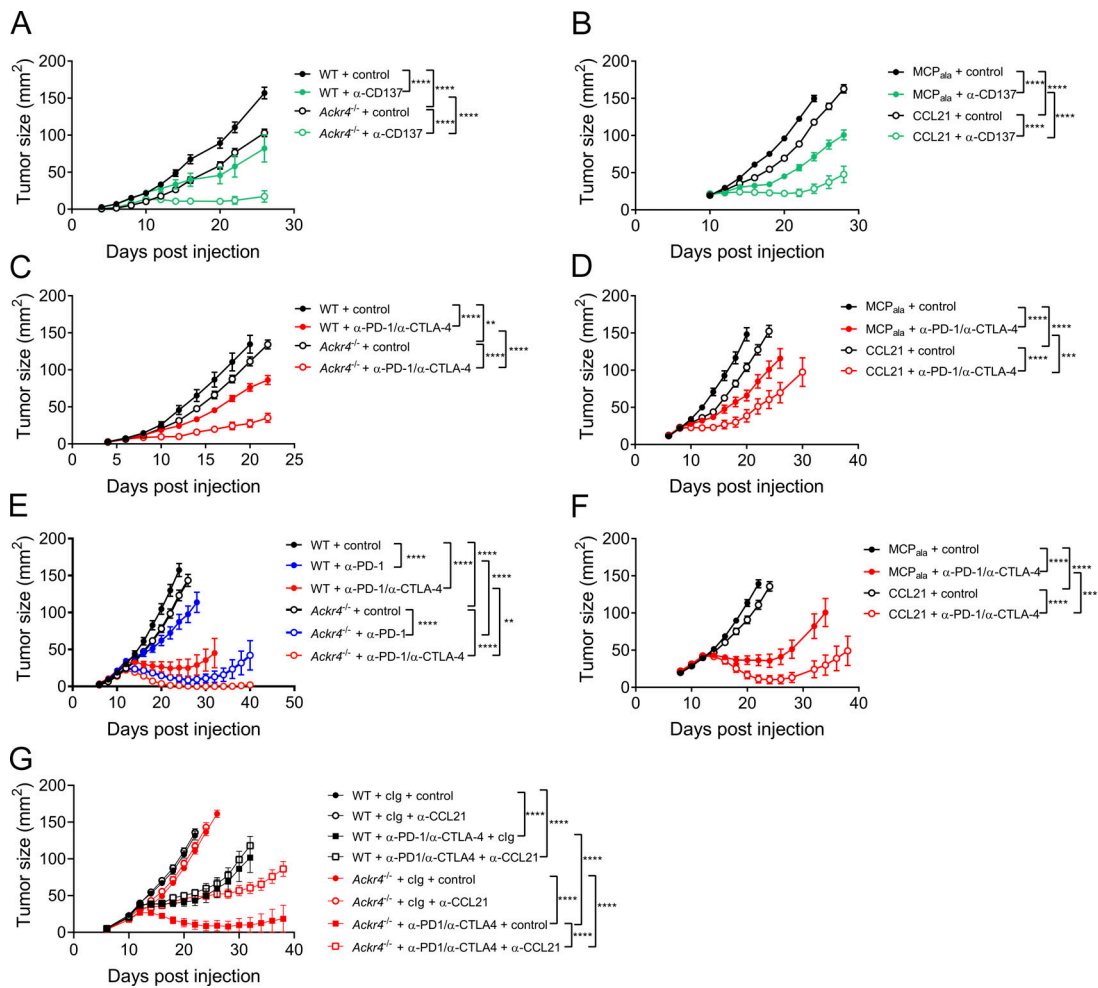


Figure 5. ACKR4 deficiency enhances responsiveness to immunotherapy. (A) Tumor growth in WT or *Ackr4*^{-/-} mice injected with 10⁵ E0771 cells and administered 100 μg anti-CD137 (clone 3H3) or rat IgG every 3 d from days 10 to 19; *n* = 7–9. (B) Tumor growth in WT mice injected with 10⁵ E0771 cells and administered MCP_{ala} or CCL21 (3 μg intratumorally) plus 100 μg anti-CD137 or rat IgG every 3 d from days 10 to 19; *n* = 5. (C) Tumor growth in WT or *Ackr4*^{-/-} mice injected with 10⁵ B16F10 cells and administered 250 μg anti-PD-1 (clone RMP1-14) and 250 μg anti-CTLA-4 (clone UC10-4F10) or 500 μg control rat/hamster Ig every 3 d from days 6 to 15; *n* = 5–6 mice. (D) Tumor growth in WT mice injected with 10⁵ B16F10 cells and administered MCP_{ala} or CCL21 (3 μg intratumorally) plus 250 μg anti-PD-1 and 250 μg anti-CTLA-4 or 500 μg control rat/hamster Ig every 3 d from days 6 to 15; *n* = 6. (E) Tumor growth curves from WT or *Ackr4*^{-/-} mice injected subcutaneously with 10⁵ MC38 cells and administered 250 μg anti-PD-1, 250 μg anti-PD-1/250 μg anti-CTLA-4, or 500 μg rat/hamster Ig every 3 d from days 12 to 21; *n* = 7–8 mice. (F) Tumor growth curves from WT mice injected subcutaneously with 10⁵ MC38 cells and administered MCP_{ala} or CCL21 (3 μg, intratumorally) plus 250 μg anti-PD-1 and 250 μg anti-CTLA-4 or 500 μg rat/hamster Ig every 3 d from days 12 to 21; *n* = 10 mice. (G) Tumor growth curves from WT or *Ackr4*^{-/-} mice injected subcutaneously with 10⁵ MC38 cells and administered 250 μg anti-PD-1 (clone RMP1-14) and 250 μg anti-CTLA-4 (clone UC10-4F10) or 500 μg rat/hamster Ig every 3 d from days 12 to 21 plus control or anti-CCL21 (100 μg) every 6 d from day -1; *n* = 6–7 mice. Data are representative from two independent experiments (A–F) or are from one experiment (G). All statistical analyses were performed using a two-way ANOVA, and data are presented as mean ± SEM. **, *P* ≤ 0.01; ***, *P* ≤ 0.001; ****, *P* ≤ 0.0001.

et al., 1998). This raises the possibility that increased levels of CCL21 in the tumor microenvironment may contribute to direct recruitment of CXCR3-expressing CD8⁺ T cells, although to date, no relationship of CXCR3 and CCL21 outside of the central nervous system has been found. These findings warrant further investigation of the potential targeting of the CCL21/ACKR4 axis to improve immunotherapy efficacy.

Materials and methods

Mice

All mice were housed at the University of Adelaide animal house or QIMR Berghofer animal house under specific pathogen-free

conditions. C57Bl/6J mice were purchased from the Animal Resource Centre (Western Australia, Australia) or Walter and Eliza Hall Institute of Medical Research and bred in-house. *Ackr4*^{-/-} mice have been previously described (Comerford et al., 2010) and were bred in-house at either the University of Adelaide or QIMR Berghofer. MMTV-PyMT⁺ and MMTV-PyMT⁺ *Ackr4*^{-/-} mice were bred in-house. All mice were backcrossed onto C57Bl/6J for a minimum of 16 generations. Experiments used age-matched and gender-matched mice between 6 and 15 wk of age, with both littermates and nonlittermates used as controls. Mice were humanely euthanized by CO₂ asphyxiation. All experiments were conducted with the approval of the University of Adelaide Animal Ethics Committee or QIMR Berghofer Animal Ethics Committee.

Cancer models

For primary tumor models, E0771 mammary carcinoma cells (10^5), E0771-OVA cells (5×10^5), MC38 colon adenocarcinoma cells (10^5), or B16F10 melanoma cells (10^5) were injected into the fourth mammary gland (E0771) or subcutaneously (MC38, B16F10). Tumor growth was measured every 2 d from days 4 to 7 using digital calipers (Mitutoyo), with tumor size calculated as the multiple of the longest tumor diameter with its perpendicular diameter. For MMTV-PyMT models, female mice were palpated twice weekly for tumor onset beginning from 8 wk of age. For fibrosarcoma models, male mice were injected subcutaneously in the hind flank with the indicated dose of MCA dissolved in 100 μ l sterile corn oil. For hematogenous metastasis models, B16F10 cells, 3LL lung carcinoma, or RM1 prostate cells were injected via the tail vein at the dose indicated in text. Lung metastasis was measured by harvesting lungs at day 14 after inoculation and enumerating metastatic nodules on the surface of the lung using a dissection microscope. For spontaneous metastasis, WT or *Ackr4*^{-/-} mice injected orthotopically into the mammary gland with 2×10^4 E0771 cells, and primary tumors were resected at day 15. Survival of mice after surgery was monitored. Cells were confirmed to be free of mycoplasma contamination by PCR analysis.

In vivo treatments

For depletion and neutralization experiments, mice were injected intraperitoneally with 100 μ g anti-CD8 β (53.5.8; BioXCell) to deplete CD8⁺ T cells, 50 μ g anti-asialoGM1 (Wako) to deplete NK cells, 250 μ g anti-IFN γ (H22; Leinco Technologies), or 100 μ g anti-CCL21 (Comerford et al., 2010) with the dosing schedule indicated in text/figure legends. For CCL21 treatments, female mice were injected into contralateral sides of the fourth mammary gland with 10^5 E0771 cells. Beginning from the day of tumor injection, mice were anesthetized and injected every 3 d with 3 μ g CCL21 or MCP_{ala}, a truncated peptide control (Kara et al., 2013; Kohler et al., 2008), into contralateral mammary glands or palpable tumors. For immunotherapy experiments, mice were injected intraperitoneally with 100 μ g anti-CD137 (3H3; BioXCell), 250 μ g anti-PD-1 (RMP1-14; BioXCell), 250 μ g anti-CTLA-4 (UC10-4F10; BioXCell), or the equivalent amount of control rat or hamster Ig in sterile PBS, in accordance with the dosing schedule in text.

Flow cytometry

Excised tumors were manually minced into small pieces and digested with 1mg ml⁻¹ collagenase IA (Sigma-Aldrich) and 30 U ml⁻¹ DNase I (Sigma-Aldrich) for 40–120 min at 37°C, with mixing every 20 min. Tumor homogenates were passed through a 70- μ m filter (BD Biosciences) and lysed of red blood cells. Inguinal LNs were excised, and single-cell suspensions obtained by pressing through a 70- μ m filter.

Single-cell suspensions were plated into round-bottom 96-well trays (Corning) at 8×10^5 – 2×10^6 cells per well, blocked with 200 μ g ml⁻¹ mouse γ -globulin (Rockland), and stained in FACS buffer (PBS + 2% FCS + 0.04% Na₂S₂O₃) with CD44 (IM7), CD8 (53–6.7), CD4 (GK1.5; RM4-5), CD3 (145-2C11), IFN- γ (XMG1.2), GzmB (GB11), Ki67 (SolA15), MHC-II (2G9), Ly6C (AL-21), CD11c

(N418) CD103 (2E7), CD172a (P84), CD45 (30-F11), CD45.2 (104), CD24 (M1/69), CD49f (GoH3), CD140a (APA5), gp38 (8.1.1), Foxp3 (MF23; FJK-17s), or NK1.1 (PK136). H-2K^b-SIINFEKL tetramers (Denton et al., 2011) were kindly provided by Professor Stephen Turner (Department of Medicine, Nursing and Health Sciences, Monash University, Clayton, Victoria, Australia) and conjugated in-house. CD1d-GalCer tetramers were kindly provided by Professor Dale Godfrey (Department of Microbiology and Immunology, The University of Melbourne, Parkville, Victoria, Australia). All antibodies were purchased from BD Biosciences, eBioscience, or BioLegend, unless otherwise stated. Biotinylated antibodies were detected by incubation with streptavidin-AF647 (BioLegend) or -BV510 (BD Biosciences). Dead cells were excluded by staining with near-infrared fixable dye diluted 1:1,000 (Life Technologies). For intracellular cytokine staining, cells were first incubated with 20 ng ml⁻¹ phorbol-12-myristate 13-acetate (Sigma-Aldrich), 1 nM ionomycin (Life Technologies), and GolgiStop (1:1,500 dilution; BD Biosciences) in complete IMDM for 4 h at 37°C. For intracellular cytokine staining or transcription factor staining, the BD Cytofix/CytoPerm kit (BD Biosciences) or the Foxp3/Transcription Factor Staining Buffer Set (Thermo Fisher Scientific) were used, respectively, according to the manufacturer's instructions. Flow cytometry data were acquired on a LSR II, FACSAria, or Fortessa (all BD Biosciences) and analyzed using FlowJo software (BD Biosciences). Cell frequencies are presented as a percentage of total viable cells, unless otherwise stated. Cell sorting experiments were performed on an Aria III (BD Biosciences).

ELISA

After digestion of E0771 tumors or naive mammary glands, protease inhibitors (Sigma-Aldrich) were added to the supernatant, which was stored at -80°C. Capture antibodies against mouse CCL19, CCL21, or CCL25 (R&D Systems) were diluted in 0.1 M NaHCO₃ and incubated at 4°C overnight. Plates were blocked with 3% BSA/PBS and incubated with tumor/mammary gland supernatant, followed by incubation with the respective biotinylated detection antibody against mouse CCL19, CCL21, or CCL25 (R&D Systems). Plates were then incubated with streptavidin-HRP (Rockland), developed with TMB Substrate solution (Thermo Fisher Scientific), stopped with 1M orthophosphoric acid, and read at 450 nm on a Biotrak II spectrophotometer (Amersham Biosciences).

BM chimeras

WT and *Ackr4*^{-/-} mice were irradiated twice with 1,050 cGy/rad and reconstituted intravenously with 5×10^6 total BM cells from WT or *Ackr4*^{-/-} donors. Mice were left for at least 8 wk to allow reconstitution before initiating experiments.

qPCR

Total RNA was extracted from sorted mammary gland cells using the RNeasy Micro Kit (Qiagen) with on-column DNase treatment and reverse-transcribed into cDNA using the Transcriptor First Strand cDNA Synthesis Kit (Roche Applied Science). qPCR was conducted using LightCycler480 SYBR Green I Master mix (Roche Applied Science) on a LightCycler480

instrument (Roche Applied Science). All procedures were performed as per the manufacturer's instructions. Cycle threshold (CT) values were determined by the second derivative method, and relative gene expression of *Ackr4* to the housekeeping gene *Rplp0* was calculated using the formula $2^{-[CT(Ackr4) - CT(Rplp0)]}$. The melting curve of each product was also analyzed to confirm the specificity of the product (*Rplp0*, forward: 5'-TGCAGA TCGGGTACCCAACCT-3', reverse: 5'-ACGCGCTTGATCCATTG A-3'; *Ackr4*, forward: 5'-AATGCTAGGTGCACTCCCATTCT-3', reverse: 5'-GCCGATTTCAGCATCTGA-3'; *Ccl21*, forward: 5'-GCA AAGAGGGAGCTAGAAAACAGA-3', reverse: 5'-TGGACGGAGGCC AGCAT-3').

TCGA analysis

All available RNA-sequencing data for primary solid tumors was downloaded from the BRCA section of the TCGA database as gene-level counts using the R package TCGAbiolinks (Colaprico et al., 2016). Genes were filtered out if their average expression was in the bottom quartile. Principal-component analysis was used to remove any outlier plates. Expression values were converted to log₂ counts per million for across samples, and expression values for *ACKR4*, *CD8A*, *IFNG*, and *PRFI* were classified as low or high based on the median expression value across samples. Survival curves were generated taking *ACKR4* high/low expression within the high expression groups for *CD8A*, *IFNG*, and *PRFI*. Pairwise comparisons were performed using the log-rank test, with P values adjusted using the Benjamini-Hochberg method.

Statistics

All statistical analyses were performed with GraphPad Prism or R. Samples sizes for sufficient statistical power were determined empirically. Significance was defined as $P < 0.05$.

Online supplemental material

Fig. S1 shows additional tumor-infiltrating lymphocytes and T cell priming in E0771 tumors. Fig. S2 shows the effect of *ACKR4* deletion on metastasis. Fig. S3 shows transcriptome analysis of human breast cancer patients from the TCGA database.

Acknowledgments

We thank Phil Darcy, Michael Kershaw, Dale Godfrey, and Andrew Brooks for reagents and the staff of Laboratory Animal Services, University of Adelaide, and QIMR for animal husbandry.

This research was funded by National Health and Medical Research Council project grants 1030247 and 1105312 to S.R. McColl and I. Comerford. M.J. Smyth was funded by National Health and Medical Research Council program grant (1132519) and senior principal research fellowship and investigator grants 1078671 and 1173958. S.R. McColl is supported by scientific research agreements with Tizona Therapeutics and Carina Biotech. M.J. Smyth has been supported by a scientific research agreement with Bristol-Myers Squibb, Aduro Biotech, and Tizona Therapeutics. S.R. McColl and M.J. Smyth are on the scientific advisory board at Tizona Therapeutics.

Author contributions: C.E. Whyte contributed to the project conceptualization, designed and performed experiments and wrote the manuscript. M. Osman, E.E. Kara, C. Abbott, J. Foeng, D.R. McKenzie, K.A. Fenix, K.L. Foyle, Y. Harata-Lee, A. Roman Aguilera, J. Hou, X. Li, I. Comerford, and M.J. Smyth performed experiments. M.A. Armstrong and S.M. Pederson performed bioinformatics analyses. S.T. Boyle and M. Kochetkova provided key reagents and methodology. I. Comerford, M.J. Smyth and S.R. McColl conceptualized the project, designed experiments, and wrote the manuscript. S.R. McColl supervised and coordinated the study.

Disclosures: Dr. Harata-Lee reported a patent number 2012903874 with royalties paid, "Tizona Therapeutics." Dr. Comerford reported a patent number 2012903874 with royalties paid, "Tizona Therapeutics." Dr. Smyth reported grants from Bristol Meyers Squibb, grants from Tizona Therapeutics, grants from Aduro Biotech, personal fees from Tizona Therapeutics, and personal fees from Compass Therapeutics outside the submitted work. In addition, Dr. Smyth had a patent number 2012903874 issued. Dr. McColl reported grants from Tizona Therapeutics, personal fees from Tizona Therapeutics, and grants from Carina Biotech outside the submitted work. In addition, Dr. McColl had a patent number 2012903874 with royalties paid, "Tizona Therapeutics." No other disclosures were reported.

Submitted: 9 April 2019

Revised: 3 February 2020

Accepted: 16 March 2020

References

- Ahern, E., M.J. Smyth, W.C. Dougall, and M.W.L. Teng. 2018. Roles of the RANKL-RANK axis in antitumor immunity - implications for therapy. *Nat. Rev. Clin. Oncol.* 15:676-693. <https://doi.org/10.1038/s41571-018-0095-y>
- Binnewies, M., A.M. Mujal, J.L. Pollack, A.J. Combes, E.A. Hardison, K.C. Barry, J. Tsui, M.K. Ruhland, K. Kersten, M.A. Abushawish, et al. 2019. Unleashing Type-2 Dendritic Cells to Drive Protective Antitumor CD4⁺ T Cell Immunity. *Cell.* 177:556-571.e16. <https://doi.org/10.1016/j.cell.2019.02.005>
- Boyle, S.T., W.V. Ingman, V. Poltavets, J.W. Faulkner, R.J. Whitfield, S.R. McColl, and M. Kochetkova. 2016. The chemokine receptor CCR7 promotes mammary tumorigenesis through amplification of stem-like cells. *Oncogene.* 35:105-115. <https://doi.org/10.1038/onc.2015.66>
- Broz, M.L., M. Binnewies, B. Boldajipour, A.E. Nelson, J.L. Pollack, D.J. Erle, A. Barczak, M.D. Rosenblum, A. Daud, D.L. Barber, et al. 2014. Dissecting the tumor myeloid compartment reveals rare activating antigen-presenting cells critical for T cell immunity. *Cancer Cell.* 26:638-652. <https://doi.org/10.1016/j.ccell.2014.09.007>
- Bryce, S.A., R.A. Wilson, E.M. Tiplady, D.L. Asquith, S.K. Bromley, A.D. Luster, G.J. Graham, and R.J. Nibbs. 2016. *ACKR4* on Stromal Cells Scavenges CCL19 To Enable CCR7-Dependent Trafficking of APCs from Inflamed Skin to Lymph Nodes. *J. Immunol.* 196:3341-3353. <https://doi.org/10.4049/jimmunol.1501542>
- Chen, D.S., and I. Mellman. 2017. Elements of cancer immunity and the cancer-immune set point. *Nature.* 541:321-330. <https://doi.org/10.1038/nature21349>
- Chester, C., M.F. Sanmamed, J. Wang, and I. Melero. 2018. Immunotherapy targeting 4-1BB: mechanistic rationale, clinical results, and future strategies. *Blood.* 131:49-57. <https://doi.org/10.1182/blood-2017-06-741041>
- Colaprico, A., T.C. Silva, C. Olsen, L. Garofano, C. Cava, D. Garolini, T.S. Sabedot, T.M. Malta, S.M. Pagnotta, I. Castiglioni, et al. 2016.

- TCGAbiolinks: an R/Bioconductor package for integrative analysis of TCGA data. *Nucleic Acids Res.* 44(8):e71. <https://doi.org/10.1093/nar/gkv1507>
- Comerford, I., S. Milasta, V. Morrow, G. Milligan, and R. Nibbs. 2006. The chemokine receptor CCX-CKR mediates effective scavenging of CCL19 in vitro. *Eur. J. Immunol.* 36:1904–1916. <https://doi.org/10.1002/eji.200535716>
- Comerford, I., R.J. Nibbs, W. Litchfield, M. Bunting, Y. Harata-Lee, S. Haylock-Jacobs, S. Forrow, H. Korner, and S.R. McColl. 2010. The atypical chemokine receptor CCX-CKR scavenges homeostatic chemokines in circulation and tissues and suppresses Th17 responses. *Blood.* 116:4130–4140. <https://doi.org/10.1182/blood-2010-01-264390>
- Costa, A., Y. Kieffer, A. Scholer-Dahirel, F. Pelon, B. Bourachot, M. Cardon, P. Sirven, I. Magagna, L. Fuhrmann, C. Bernard, et al. 2018. Fibroblast Heterogeneity and Immunosuppressive Environment in Human Breast Cancer. *Cancer Cell.* 33:463–479.e10. <https://doi.org/10.1016/j.ccell.2018.01.011>
- de Mingo Pulido, Á., A. Gardner, S. Hiebler, H. Soliman, H.S. Rugo, M.F. Krummel, L.M. Coussens, and B. Ruffell. 2018. TIM-3 Regulates CD103⁺ Dendritic Cell Function and Response to Chemotherapy in Breast Cancer. *Cancer Cell.* 33:60–74.e6. <https://doi.org/10.1016/j.ccell.2017.11.019>
- Denkert, C., C. Liedtke, A. Tutt, and G. von Minckwitz. 2017. Molecular alterations in triple-negative breast cancer—the road to new treatment strategies. *Lancet.* 389:2430–2442. [https://doi.org/10.1016/S0140-6736\(16\)32454-0](https://doi.org/10.1016/S0140-6736(16)32454-0)
- Denton, A.E., R. Wesselingh, S. Gras, C. Guillonau, M.R. Olson, J.D. Mintern, W. Zeng, D.C. Jackson, J. Rossjohn, P.D. Hodgkin, et al. 2011. Affinity thresholds for naive CD8⁺ CTL activation by peptides and engineered influenza A viruses. *J. Immunol.* 187:5733–5744. <https://doi.org/10.4049/jimmunol.1003937>
- Fantozzi, A., and G. Christofori. 2006. Mouse models of breast cancer metastasis. *Breast Cancer Res.* 8:212. <https://doi.org/10.1186/bcr1530>
- Feng, L.Y., Z.L. Ou, F.Y. Wu, Z.Z. Shen, and Z.M. Shao. 2009. Involvement of a novel chemokine decoy receptor CCX-CKR in breast cancer growth, metastasis and patient survival. *Clin. Cancer Res.* 15:2962–2970. <https://doi.org/10.1158/1078-0432.CCR-08-2495>
- Fourcade, J., Z. Sun, M. Benallaoua, P. Guillaume, I.F. Luescher, C. Sander, J.M. Kirkwood, V. Kuchroo, and H.M. Zarour. 2010. Upregulation of Tim-3 and PD-1 expression is associated with tumor antigen-specific CD8⁺ T cell dysfunction in melanoma patients. *J. Exp. Med.* 207:2175–2186. <https://doi.org/10.1084/jem.20100637>
- Galon, J., A. Costes, F. Sanchez-Cabo, A. Kirilovsky, B. Mlecnik, C. Lagorce-Pagès, M. Tosolini, M. Camus, A. Berger, P. Wind, et al. 2006. Type, density, and location of immune cells within human colorectal tumors predict clinical outcome. *Science.* 313:1960–1964. <https://doi.org/10.1126/science.1129139>
- Haniffa, M., A. Shin, V. Bigley, N. McGovern, P. Teo, P. See, P.S. Wasan, X.N. Wang, F. Malinarich, B. Malleret, et al. 2012. Human tissues contain CD141hi cross-presenting dendritic cells with functional homology to mouse CD103⁺ nonlymphoid dendritic cells. *Immunity.* 37:60–73. <https://doi.org/10.1016/j.immuni.2012.04.012>
- Harata-Lee, Y., M.E. Turvey, J.A. Brazzatti, C.E. Gregor, M.P. Brown, M.J. Smyth, I. Comerford, and S.R. McColl. 2014. The atypical chemokine receptor CCX-CKR regulates metastasis of mammary carcinoma via an effect on EMT. *Immunol. Cell Biol.* 92:815–824. <https://doi.org/10.1038/icb.2014.58>
- Heinzel, K., C. Benz, and C.C. Bleul. 2007. A silent chemokine receptor regulates steady-state leukocyte homing in vivo. *Proc. Natl. Acad. Sci. USA.* 104:8421–8426. <https://doi.org/10.1073/pnas.0608274104>
- Herbst, R.S., J.C. Soria, M. Kowanetz, G.D. Fine, O. Hamid, M.S. Gordon, J.A. Sosman, D.F. McDermott, J.D. Powderly, S.N. Gettinger, et al. 2014. Predictive correlates of response to the anti-PD-L1 antibody MPDL3280A in cancer patients. *Nature.* 515:563–567. <https://doi.org/10.1038/nature14011>
- Hildner, K., B.T. Edelson, W.E. Purtha, M. Diamond, H. Matsushita, M. Kohyama, B. Calderon, B.U. Schraml, E.R. Unanue, M.S. Diamond, et al. 2008. Batf3 deficiency reveals a critical role for CD8α⁺ dendritic cells in cytotoxic T cell immunity. *Science.* 322:1097–1100. <https://doi.org/10.1126/science.1164206>
- Johnstone, C.N., Y.E. Smith, Y. Cao, A.D. Burrows, R.S. Cross, X. Ling, R.P. Redvers, J.P. Doherty, B.L. Eckhardt, A.L. Natoli, et al. 2015. Functional and molecular characterisation of EO771.LMB tumours, a new C57BL/6-mouse-derived model of spontaneously metastatic mammary cancer. *Dis. Model. Mech.* 8:237–251. <https://doi.org/10.1242/dmm.017830>
- Kara, E.E., I. Comerford, C.R. Bastow, K.A. Fenix, W. Litchfield, T.M. Handel, and S.R. McColl. 2013. Distinct chemokine receptor axes regulate Th9 cell trafficking to allergic and autoimmune inflammatory sites. *J. Immunol.* 191:1110–1117. <https://doi.org/10.4049/jimmunol.1203089>
- Kara, E.E., C.R. Bastow, D.R. McKenzie, C.E. Gregor, K.A. Fenix, R. Babb, T.S. Norton, D. Zotos, L.B. Rodda, J.R. Hermes, et al. 2018. Atypical chemokine receptor 4 shapes activated B cell fate. *J. Exp. Med.* 215:801–813. <https://doi.org/10.1084/jem.20171067>
- Kohler, R.E., I. Comerford, S. Townley, S. Haylock-Jacobs, I. Clark-Lewis, and S.R. McColl. 2008. Antagonism of the chemokine receptors CXCR3 and CXCR4 reduces the pathology of experimental autoimmune encephalomyelitis. *Brain Pathol.* 18:504–516.
- Kurtulus, S., A. Madi, G. Escobar, M. Klapholz, J. Nyman, E. Christian, M. Pawlak, D. Dionne, J. Xia, O. Rozenblatt-Rosen, et al. 2019. Checkpoint Blockade Immunotherapy Induces Dynamic Changes in PD-1⁺CD8⁺ Tumor-Infiltrating T Cells. *Immunity.* 50:181–194.e6. <https://doi.org/10.1016/j.immuni.2018.11.014>
- Lin, E.Y., J.G. Jones, P. Li, L. Zhu, K.D. Whitney, W.J. Muller, and J.W. Pollard. 2003. Progression to malignancy in the polyoma middle T oncoprotein mouse breast cancer model provides a reliable model for human diseases. *Am. J. Pathol.* 163:2113–2126. [https://doi.org/10.1016/S0002-9440\(10\)63568-7](https://doi.org/10.1016/S0002-9440(10)63568-7)
- Lucas, B., A.J. White, M.H. Ulvmar, R.J. Nibbs, K.M. Sitnik, W.W. Agace, W.E. Jenkinson, G. Anderson, and A. Rot. 2015. CCR1/ACKR4 is expressed in key thymic microenvironments but is dispensable for T lymphopoiesis at steady state in adult mice. *Eur. J. Immunol.* 45:574–583. <https://doi.org/10.1002/eji.201445015>
- Matsuzaki, J., S. Gnajatic, P. Mhawech-Fauceglia, A. Beck, A. Miller, T. Tsuji, C. Eppolito, F. Qian, S. Lele, P. Shrikant, et al. 2010. Tumor-infiltrating NY-ESO-1-specific CD8⁺ T cells are negatively regulated by LAG-3 and PD-1 in human ovarian cancer. *Proc. Natl. Acad. Sci. USA.* 107:7875–7880. <https://doi.org/10.1073/pnas.1003345107>
- Melero, I., W.W. Shuford, S.A. Newby, A. Aruffo, J.A. Ledbetter, K.E. Hellström, R.S. Mittler, and L. Chen. 1997. Monoclonal antibodies against the 4-1BB T-cell activation molecule eradicate established tumors. *Nat. Med.* 3:682–685. <https://doi.org/10.1038/nm0697-682>
- Mikucki, M.E., D.T. Fisher, J. Matsuzaki, J.J. Skitzki, N.B. Gaulin, J.B. Muhitch, A.W. Ku, J.G. Frelinger, K. Odunsi, T.F. Gajewski, et al. 2015. Non-redundant requirement for CXCR3 signalling during tumoricidal T-cell trafficking across tumour vascular checkpoints. *Nat. Commun.* 6:7458. <https://doi.org/10.1038/ncomms8458>
- Ngiwo, S.F., S. Loi, D. Thomas, and M.J. Smyth. 2016. Mouse Models of Tumor Immunotherapy. *Adv. Immunol.* 130:1–24. <https://doi.org/10.1016/bs.ai.2015.12.004>
- Ohl, L., M. Mohaupt, N. Czeloth, G. Hintzen, Z. Kiafard, J. Zwirner, T. Blankenstein, G. Henning, and R. Förster. 2004. CCR7 governs skin dendritic cell migration under inflammatory and steady-state conditions. *Immunity.* 21:279–288. <https://doi.org/10.1016/j.immuni.2004.06.014>
- Pagès, F., A. Kirilovsky, B. Mlecnik, M. Asslaber, M. Tosolini, G. Bindea, C. Lagorce, P. Wind, F. Marliot, P. Bruneval, et al. 2009. In situ cytotoxic and memory T cells predict outcome in patients with early-stage colorectal cancer. *J. Clin. Oncol.* 27:5944–5951. <https://doi.org/10.1200/JCO.2008.19.6147>
- Peske, J.D., E.D. Thompson, L. Gemta, R.A. Baylis, Y.X. Fu, and V.H. Engelhard. 2015. Effector lymphocyte-induced lymph node-like vasculature enables naive T-cell entry into tumours and enhanced anti-tumour immunity. *Nat. Commun.* 6:7114. <https://doi.org/10.1038/ncomms8114>
- Rappert, A., K. Biber, C. Nolte, M. Lipp, A. Schubel, B. Lu, N.P. Gerard, C. Gerard, H.W. Boddeke, and H. Kettenmann. 2002. Secondary lymphoid tissue chemokine (CCL21) activates CXCR3 to trigger a Cl⁻ current and chemotaxis in murine microglia. *J. Immunol.* 168:3221–3226. <https://doi.org/10.4049/jimmunol.168.7.3221>
- Roberts, E.W., M.L. Broz, M. Binnewies, M.B. Headley, A.E. Nelson, D.M. Wolf, T. Kaisho, D. Bogunovic, N. Bhardwaj, and M.F. Krummel. 2016. Critical Role for CD103(+)/CD141(+) Dendritic Cells Bearing CCR7 for Tumor Antigen Trafficking and Priming of T Cell Immunity in Melanoma. *Cancer Cell.* 30:324–336. <https://doi.org/10.1016/j.ccell.2016.06.003>
- Saijo, N., A. Ozaki, Y. Beppu, K. Takahashi, J. Fujita, Y. Sasaki, H. Nomori, M. Kimata, E. Shimizu, and A. Hoshi. 1984. Analysis of metastatic spread and growth of tumor cells in mice with depressed natural killer activity by anti-asialo GM1 antibody or anticancer agents. *J. Cancer Res. Clin. Oncol.* 107:157–163. <https://doi.org/10.1007/BF01032600>
- Sakuishi, K., L. Apetoh, J.M. Sullivan, B.R. Blazyn, V.K. Kuchroo, and A.C. Anderson. 2010. Targeting Tim-3 and PD-1 pathways to reverse T cell

- exhaustion and restore anti-tumor immunity. *J. Exp. Med.* 207: 2187–2194. <https://doi.org/10.1084/jem.20100643>
- Sharma, S., M. Stolina, J. Luo, R.M. Strieter, M. Burdick, L.X. Zhu, R.K. Batra, and S.M. Dubinett. 2000. Secondary lymphoid tissue chemokine mediates T cell-dependent antitumor responses in vivo. *J. Immunol.* 164: 4558–4563. <https://doi.org/10.4049/jimmunol.164.9.4558>
- Sharma, S., S.C. Yang, S. Hillinger, L.X. Zhu, M. Huang, R.K. Batra, J.F. Lin, M.D. Burdick, R.M. Strieter, and S.M. Dubinett. 2003. SLC/CCL21-mediated anti-tumor responses require IFN γ , MIG/CXCL9 and IP-10/CXCL10. *Mol. Cancer.* 2:22. <https://doi.org/10.1186/1476-4598-2-22>
- Shi, J.Y., L.X. Yang, Z.C. Wang, L.Y. Wang, J. Zhou, X.Y. Wang, G.M. Shi, Z.B. Ding, A.W. Ke, Z. Dai, et al. 2015. CC chemokine receptor-like 1 functions as a tumour suppressor by impairing CCR7-related chemotaxis in hepatocellular carcinoma. *J. Pathol.* 235:546–558. <https://doi.org/10.1002/path.4450>
- Soto, H., W. Wang, R.M. Strieter, N.G. Copeland, D.J. Gilbert, N.A. Jenkins, J. Hedrick, and A. Zlotnik. 1998. The CC chemokine 6Ckine binds the CXCR3 chemokine receptor CXCR3. *Proc. Natl. Acad. Sci. USA.* 95:8205–8210. <https://doi.org/10.1073/pnas.95.14.8205>
- Spranger, S., R. Bao, and T.F. Gajewski. 2015. Melanoma-intrinsic β -catenin signalling prevents anti-tumour immunity. *Nature.* 523:231–235. <https://doi.org/10.1038/nature14404>
- Spranger, S., D. Dai, B. Horton, and T.F. Gajewski. 2017. Tumor-Residing Batf3 Dendritic Cells Are Required for Effector T Cell Trafficking and Adoptive T Cell Therapy. *Cancer Cell.* 31:711–723.e4. <https://doi.org/10.1016/j.ccell.2017.04.003>
- Takeda, K., M. Nakayama, M. Sakaki, Y. Hayakawa, M. Imawari, K. Ogasawara, K. Okumura, and M.J. Smyth. 2011. IFN- γ production by lung NK cells is critical for the natural resistance to pulmonary metastasis of B16 melanoma in mice. *J. Leukoc. Biol.* 90:777–785. <https://doi.org/10.1189/jlb.0411208>
- Tal, O., H.Y. Lim, I. Gurevich, I. Milo, Z. Shipony, L.G. Ng, V. Angeli, and G. Shakhar. 2011. DC mobilization from the skin requires docking to immobilized CCL21 on lymphatic endothelium and intralymphatic crawling. *J. Exp. Med.* 208:2141–2153. <https://doi.org/10.1084/jem.20102392>
- Townson, J.R., and R.J. Nibbs. 2002. Characterization of mouse CCX-CKR, a receptor for the lymphocyte-attracting chemokines TECK/mCCL25, SLC/mCCL21 and MIP-3 β /mCCL19: comparison to human CCX-CKR. *Eur. J. Immunol.* 32:1230–1241. [https://doi.org/10.1002/1521-4141\(200205\)32:5<1230::AID-IMMU1230>3.0.CO;2-L](https://doi.org/10.1002/1521-4141(200205)32:5<1230::AID-IMMU1230>3.0.CO;2-L)
- Tumeh, P.C., C.L. Harview, J.H. Yearley, I.P. Shintaku, E.J. Taylor, L. Robert, B. Chmielowski, M. Spasic, G. Henry, V. Ciobanu, et al. 2014. PD-1 blockade induces responses by inhibiting adaptive immune resistance. *Nature.* 515:568–571. <https://doi.org/10.1038/nature13954>
- Turley, S.J., V. Cremasco, and J.L. Astarita. 2015. Immunological hallmarks of stromal cells in the tumour microenvironment. *Nat. Rev. Immunol.* 15: 669–682. <https://doi.org/10.1038/nri3902>
- Ulvmar, M.H., K. Werth, A. Braun, P. Kelay, E. Hub, K. Eller, L. Chan, B. Lucas, I. Novitzky-Basso, K. Nakamura, et al. 2014. The atypical chemokine receptor CCRL1 shapes functional CCL21 gradients in lymph nodes. *Nat. Immunol.* 15:623–630. <https://doi.org/10.1038/ni.2889>
- Wang, J., X. Zhang, S.M. Thomas, J.R. Grandis, A. Wells, Z.G. Chen, and R.L. Ferris. 2005. Chemokine receptor 7 activates phosphoinositide-3 kinase-mediated invasive and pro-survival pathways in head and neck cancer cells independent of EGFR. *Oncogene.* 24:5897–5904. <https://doi.org/10.1038/sj.onc.1208740>
- Weber, M., R. Hauschild, J. Schwarz, C. Moussion, I. de Vries, D.F. Legler, S.A. Luther, T. Bollenbach, and M. Sixt. 2013. Interstitial dendritic cell guidance by haptotactic chemokine gradients. *Science.* 339:328–332. <https://doi.org/10.1126/science.1228456>
- Woo, S.R., M.E. Turnis, M.V. Goldberg, J. Bankoti, M. Selby, C.J. Nirschl, M.L. Bettini, D.M. Gravano, P. Vogel, C.L. Liu, et al. 2012. Immune inhibitory molecules LAG-3 and PD-1 synergistically regulate T-cell function to promote tumoral immune escape. *Cancer Res.* 72:917–927. <https://doi.org/10.1158/0008-5472.CAN-11-1620>

Supplemental material

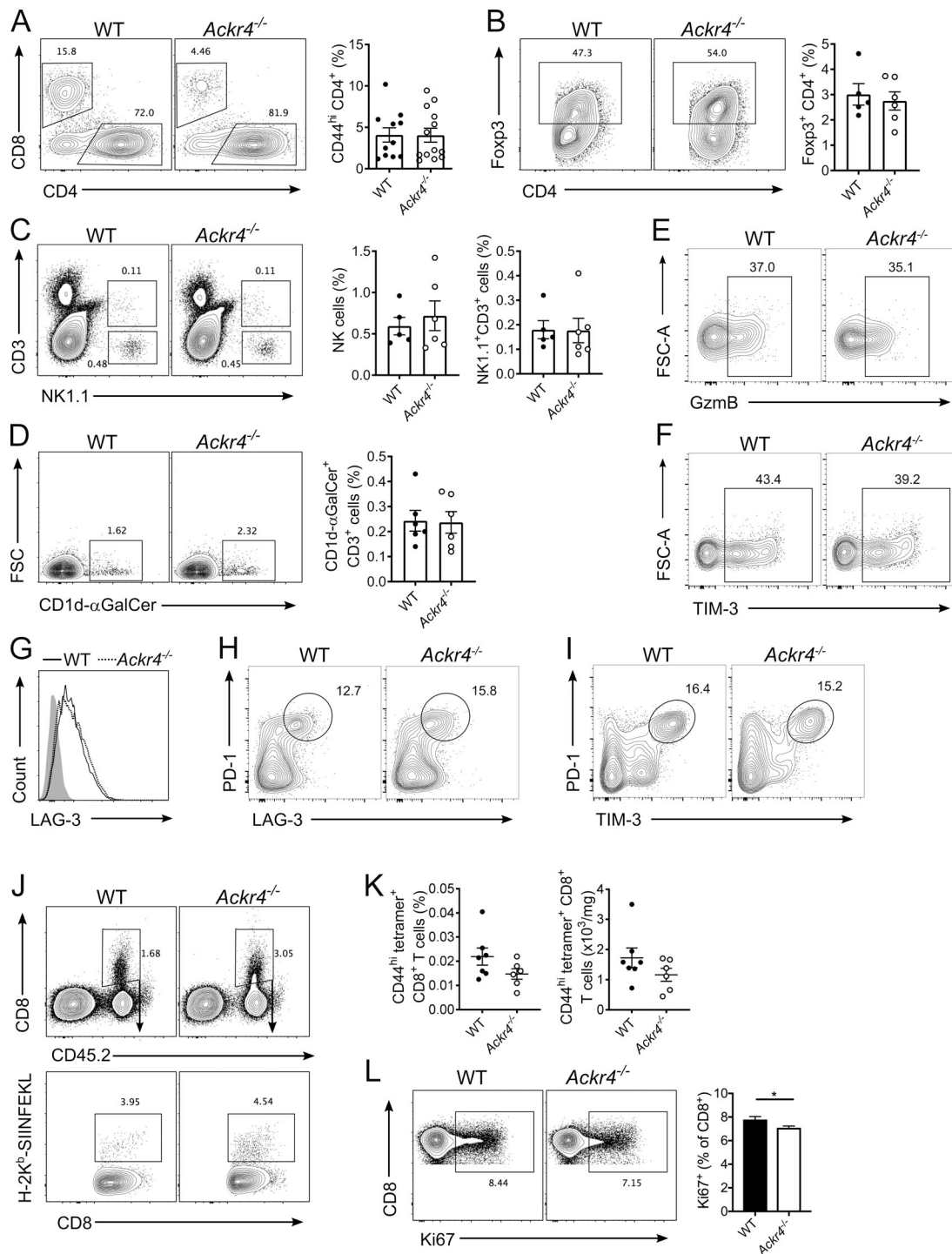


Figure S1. **Tumor-infiltrating lymphocytes and CD8⁺ T cell priming in mice bearing E0771 tumors.** (A–G) WT or *Ackr4*^{-/-} mice were injected with 10⁵ E0771 cells into the fourth mammary gland and analyzed 18–21 d after injection. (A) Representative gating and frequency (of total viable cells) of intratumor CD44^{hi} CD4⁺ T cells; *n* = 11–13. (B) Representative gating and frequency of intratumor Foxp3⁺ regulatory t cells. *n* = 5–6. (C) Representative gating and frequency of intratumor NK cells and NK1.1⁺ CD3⁺ NKT cells. *n* = 5–6. (D) Representative gating and frequency of type I invariant NKT cells. *n* = 5–6. FSC, forward scatter. (E–H) Representative gating strategy of intratumor CD8⁺ T cells for (E) granzyme B, (F) TIM-3, (G) LAG-3, (H) PD-1⁺ LAG-3⁺, and (I) PD-1⁺ TIM-3⁺ (data in Fig. 2, C and E–G). (J) Representative gating strategy of OVA-specific CD8⁺ T cells in E0771-OVA tumors (data in Fig. 2 F). (K) Frequency and number of OVA-specific CD44^{hi} CD8⁺ T cells in dLNs of mice injected with 5 × 10⁵ E0771-OVA cells; *n* = 6–7. (L) Representative gating and frequency of Ki67 expression on CD8⁺ T cells in the dLNs of mice injected with 10⁵ E0771 cells. *n* = 10, unpaired *t* test. Data representative of at least two independent experiments. Data are presented as mean ± SEM. *, *P* ≤ 0.05.

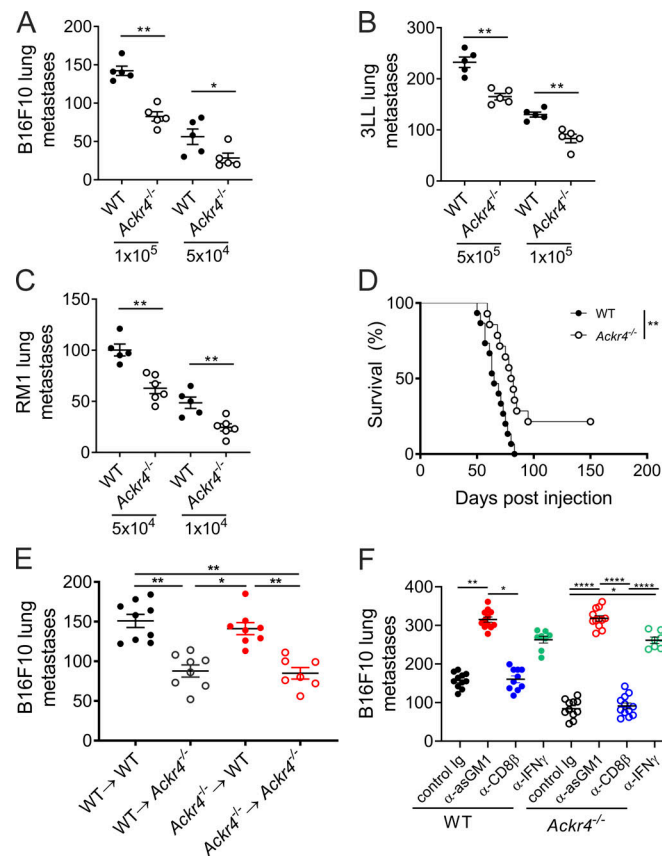


Figure S2. **Loss of nonhematopoietic ACKR4 inhibits tumor metastasis.** (A–C) WT or *Acker4*^{-/-} mice were intravenously injected with (A) B16F10 melanoma, (B) 3LL lung carcinoma, or (C) RM1 prostate cells, and the number of lung metastases were counted ($n = 5–6$ mice, Mann–Whitney test). (D) Survival curve of WT or *Acker4*^{-/-} mice injected with 2×10^4 E0771 cells, with primary tumors resected at day 15 ($n = 14–15$, Mantel–Cox test). (E) Lung metastasis in BM chimeras of WT and *Acker4*^{-/-} mice (donor BM→host). Mice were injected with 10^5 B16F10 cells, lungs were harvested 14 d after inoculation, and colonies were counted ($n = 7–9$, Kruskal–Wallis test). (F) WT or *Acker4*^{-/-} mice were injected with 10^5 B16F10 cells, lungs were harvested 14 d after inoculation, and colonies were counted ($n = 7–9$, Kruskal–Wallis test). (F) WT or *Acker4*^{-/-} mice were injected with 10^5 B16F10 cells, lungs were harvested 14 d after inoculation, and colonies were counted ($n = 7–9$, Kruskal–Wallis test). (F) WT or *Acker4*^{-/-} mice were injected with 10^5 B16F10 cells, lungs were harvested 14 d after inoculation, and colonies were counted ($n = 7–9$, Kruskal–Wallis test). Data are pooled from two independent experiments and presented as mean \pm SEM. *, $P \leq 0.05$; **, $P \leq 0.01$; ****, $P \leq 0.0001$.

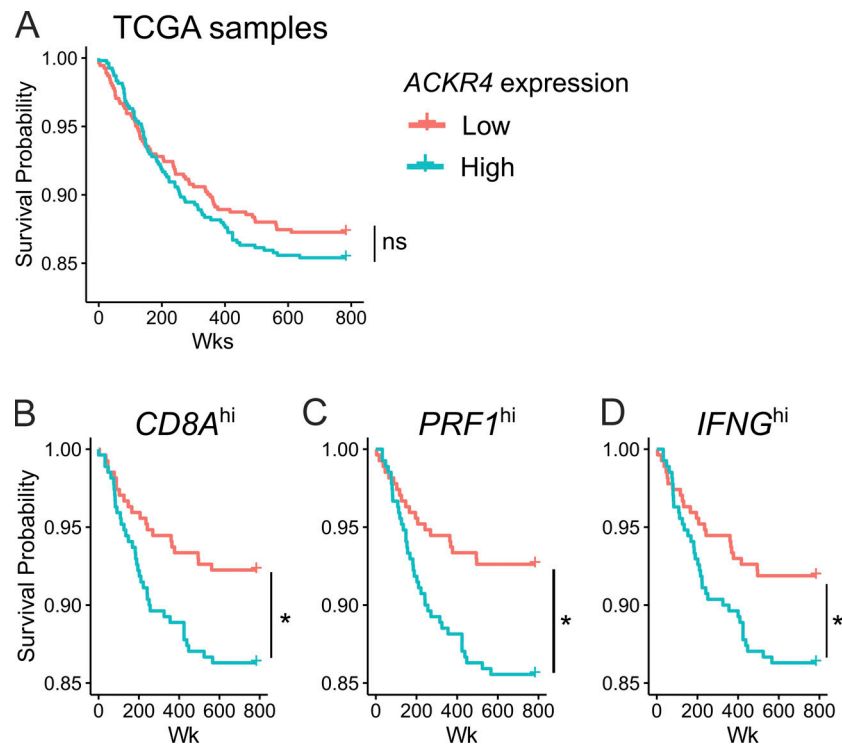


Figure S3. **Low ACKR4 expression correlates with increased survival in stratified patient groups.** (A) Survival curves from TCGA analyses of patients with breast-invasive carcinoma stratified by ACKR4 expression, with the median log counts per million value across all samples as the boundary between low and high expression. (B–D) Survival curves from patients with high expression of (B) CD8A, (C) PRF1, or (D) IFNG stratified by ACKR4 expression; $n = 1,085$, pairwise comparisons by log-rank test, adjusted with Benjamini–Hochberg method. *, $P \leq 0.05$; ns, $P > 0.05$.